Clinical Ophthalmology

Dovepress
open access to scientific and medical research

Open Access Full Text Article

ORIGINAL RESEARCH

Scheimpflug-Based Corneal Biomechanical Analysis As A Predictor of Glaucoma in Eyes With High Myopia

Pedro ML Baptista[1,2], André S Ferreira[1,3], Nisa P Silva[1], Ana RM Figueiredo[1], Isabel C Sampaio[1], Rita VF Reis[1], Renato Ambrósio Jr[4–8], Pedro M A M Menéres[1,2], João N M Beirão[1,2], Maria J F S Menéres[1,2]

[1]Ophthalmology Department, Centro Hospitalar Universitário do Porto, Porto, Portugal; [2]Instituto de Ciências Biomédicas Abel Salazar, Universidade do Porto, Porto, Portugal; [3]Faculdade de Medicina da Universidade do Porto, Universidade do Porto, Porto, Portugal; [4]Rio de Janeiro Corneal Tomography and Biomechanics Study Group, Rio de Janeiro, RJ, Brazil; [5]Department of Cornea and Refractive Surgery, Instituto de Olhos Renato Ambrósio, Rio de Janeiro, Brazil; [6]Department of Ophthalmology, Federal University of the State of Rio de Janeiro (UNIRIO), Rio de Janeiro, Brazil; [7]Federal University of São Paulo (UNIFESP), São Paulo, Brazil; [8]Brazilian Study Group of Artificial Intelligence and Corneal Analysis - BrAIN, Rio de Janeiro & Maceió, Brazil

Correspondence: Pedro ML Baptista, Centro Hospitalar Universitário do Porto, Largo Prof. Abel Salazar 4099-001 Porto, Portugal, Email pedroyybaptista@gmail.com

Purpose: To address if corneal biomechanical behavior has a predictive value for the presence of glaucomatous optical neuropathy in eyes with high myopia.

Patients and Methods: This observational cross-sectional study included 209 eyes from 108 consecutive patients, divided into four groups: high myopia and primary open-angle glaucoma (POAG) – HMG, n = 53; high myopia without POAG – HMNG, n = 53; non-myopic with POAG – POAG, n = 50; non-myopic and non-POAG– NMNG, n = 53. Biomechanical assessment was made through a Scheimpflug-camera-based technology. Receiver operating characteristic curves were made for the discrimination between groups. Multivariable logistic regression models were performed to address the predictive value of corneal biomechanics for the presence of glaucoma.

Results: Areas Under the Receiver Operating Characteristic (AUROCs) above 0.6 were found in 6 parameters applied to discriminate between HMG and HMNG and six parameters to discriminate between POAG and NMNG. The biomechanical models with the highest power of prediction for the presence of glaucoma included 5 parameters with an AUROC of 0.947 for eyes with high myopia and 6 parameters with an AUROC of 0.857 for non-myopic eyes. In the final model, including all eyes, and adjusted for the presence of high myopia, the highest power of prediction for the presence of glaucoma was achieved including eight biomechanical parameters, with an AUROC of 0.917.

Conclusion: Corneal biomechanics demonstrated differences in eyes with glaucoma and mainly in myopic eyes. A biomechanical model based on multivariable logistic regression analysis and adjusted for high myopia was built, with an overall probability of 91.7% for the correct prediction of glaucomatous damage.

Plain Language Summary: High myopia and glaucoma are two entities with a worldwide growing prevalence and with a great visual, social and economic impact. High myopic eyes have a greater risk of glaucomatous damage, but early diagnosis is difficult due to the particularities of the eyes. This study asks if corneal biomechanics assessment can have a role in the risk prediction of glaucomatous damage in eyes with high myopia. As a strong biomechanical model for the correct prediction of glaucomatous damage was built, corneal biomechanics study can be a useful tool in the management of high myopic eyes with suspected glaucoma.

Keywords: corneal biomechanics, corvis, glaucoma, high myopia, intraocular pressure, Scheimpflug camera

Introduction

Glaucoma is the leading cause of irreversible blindness worldwide, affecting more than 70 million of people and estimated to affect about 110 million in 2040.[1]

Received: 21 September 2023
Accepted: 4 January 2024
Published: 22 February 2024

Progressive and permanent vision loss results from optic nerve damage and loss of retinal ganglion cells (RGC). Effective and continuous reduction of intraocular pressure (IOP) remains the only proven method to prevent and delay the progression of glaucomatous visual impairment.[2] However, the irreversible injury of the optic nerve, gradual narrowing of the visual field and progressive loss of visual function despite average IOP below normal levels (normotensive glaucoma) suggests that other important factors may play a role.[3]

As the lamina cribrosa is the primary location of damage to retinal nerve fibers, according to the mechanical hypothesis of glaucoma, growing evidence suggests that biomechanical factors are involved in its pathogenesis.[4–8] In this sense, recent studies suggested that the biomechanical properties of sclera and scleral lamina cribrosa (LC) determine biomechanical changes of the optic nerve head (ONH),[9,10] thus playing an important role in the pathologic process of the RGC loss and contributing to optic nerve damage.[11–13] Since the cornea and sclera are continuous collagenous sheaths made up of similar extracellular matrix constituents, it can be hypothesized that the biomechanical properties of the cornea may be somehow related to those of LC or peripapillary sclera, influencing the response of the ONH to IOP and the subsequent amount of axonal nerve damage.[14] In highly myopic eyes, the ONH is tilted and the LC is significantly thinner than in non-highly myopic, which can increase the translaminar pressure gradient at each given intraocular pressure and may explain the increased susceptibility to glaucoma in these patients.[15,16]

Introduced at the AAO meeting in 2010, the Corvis ST® (Oculus, Wetzlar, Germany), is a non-contact tonometer system with a collimated air pulse with consistent pressure profile that acquires 4300 frames/s using a UHS Scheimpflug camera with ultraviolet-free 455 nm blue light, covering 8.5 mm horizontally of a single slit to allow evaluation of corneal deformation.[17] In addition to the measurement of several dynamic corneal response parameters (DCRs), this technology was validated by Vinciguerra et al[18–20] to produce IOP measurements with reduced biomechanical effect in the form of biomechanically corrected IOP (bIOP).

To the authors' best knowledge, the role of corneal biomechanics assessment in the subset of eyes with high myopia and glaucoma is not established. We hypothesized that Scheimpflug-camera-derived corneal biomechanical assessment can have a predictive value for the presence of glaucomatous damage in eyes with high myopia.

Materials and Methods

Design

An observational cross-sectional case–control study. The study adhered to the tenets of the Declaration of Helsinki. Approval was obtained from the "Departamento de Ensino, Formação e Investigação" (DEFI), nr: 130-DEFI-132-CE. The informed consent from the patients was waived due to the total anonymization and confidentiality of the data and the absence of detailed individual data.

Population

Two-hundred and nine eyes from 108 consecutive patients.

Group Formation / Inclusion and Exclusion Criteria

The eyes were divided into four groups: eyes with high myopia and primary open-angle glaucoma (POAG) – HMG, n = 53; eyes with high myopia without POAG – HMNG, n = 53; non-myopic eyes with POAG – POAG, n = 50; non-myopic and non-POAG eyes – NMNG, n = 53.

High myopia was defined as a negative manifest refraction spherical equivalent (MRSE) ≥−6D or an axial length (AL) ≥26mm. POAG was defined by optic disc appearance (presence of neuroretinal rim thinning, excavation, notching, or characteristic retinal nerve fiber layer defect) based on slit lamp fundus stereoscopic examination, corresponding or typical glaucomatous visual field abnormality, gonioscopically open angle, and absence of secondary cause of IOP elevation. Visual field abnormality was based on Anderson and Patella criteria[21] of one or more of the following: a cluster of three or more non-edge points with a P value of less than 5%, including 1 point or more with a P value of less than 1%, on the pattern deviation map in at least one hemifield; a pattern SD with a P value of less than 5%; or glaucoma

hemifield test results outside the normal limits. NMNG eyes had an untreated GAT-IOP lower than 21 mm Hg, healthy discs, and no ocular pathologies.

Exclusion criteria were contact lens use, ocular conditions that could mimic glaucomatous visual field loss particularly congenital or acquired optic nerve diseases, history of glaucoma surgical procedures, corneal dystrophies or ectatic diseases, and previous trauma or corneal scarring.

Demographic and Clinical Data

Data were recorded regarding age, gender, manifest refraction spherical equivalent (MRSE), pachymetry-adjusted[22] Goldmann applanation tonometry-intraocular pressure (GAT-IOP, mmHg), and the number of IOP lowering drops taken. All information from personal and family history, slit lamp examination and fundoscopy was analyzed.

Anatomic Data

Within the glaucomatous eye groups (HMG and POAG), data was collected regarding the peripapillary retinal nerve fiber layer thickness (ppRNFLT, µm, 3.5mm ring) mean value (M), and each of the six sector values – inferior nasal (IN), inferior temporal (IT), superior nasal (SN), superior temporal (ST), nasal (N) and temporal (T) – measured by spectral domain optical coherence tomography (SD-OCT, Spectralis, Heidelberg®) and regarding optical biometry derived axial length (AL, mm, IOL Master, Zeiss®). In cases of inaccurate or impossible segmentation due to typical myopic disc dysgenesis (33 eyes in the HMG) and with clearly visible very thinned ppRNFL, the floor value of 25µm was introduced, in order to make the statistical analysis possible.

Visual Field

Visual field (VF) was assessed in the glaucomatous eye groups (HMG and POAG) by means of standard automated perimetry (SAP) with the *Sita-fast* strategy in the 30–2 test pattern of the Zeiss-Humphrey Field Analyzer 3®, and data were collected regarding Glaucoma Hemifield Test (GHT), Visual Field Index (VFI), Mean Deviation (MD) and Pattern Standard Deviation (PSD). Only reliable exams were included (cutoff of 33% false positive or false negative and a cutoff of 20% for fixation losses).

Corneal Biomechanics

The analysis was made through the DCR parameters from the Scheimpflug-camera-based analysis (Corvis-ST, OCULUS®). Only exams with "OK" quality score were included. Parameters from the three major timepoints were recorded: time from the initiation of air puff until the first applanation (A1T), second applanation (A2T) and highest concavity (HCT). Additional 1st generation parameters from the maximum deformation on the oscillatory phase (Max) and from Whole Eye Movement (WEM) were analyzed along with the biomechanically corrected IOP (bIOP) and the composed 2nd generation parameters, including Corvis Biomechanical Index (CBI), Stiffness Parameter in A1 (SP-A1) and Stress-Strain Index (SS-I). Pachymetry assessment was made through the Corvis-derived central corneal thickness (cCCT). The Dynamic Corneal Response Layout, with different timepoints of the exam and several parameters is shown in Figure 1, and all Scheimpflug-based parameters used in the study and its explanation are summarised in Table 1.

Statistical Analysis

The normality of the data was tested with the Shapiro–Wilk and Kolmogorov–Smirnov tests. When parametric analysis could be applied, the Student's *t*-test was used to compare the variables. When nonparametric tests were needed, the Wilcoxon rank-sum test was applied. The $\chi 2$ was used to compare nominal and ordinal variables.

Descriptive statistics of all dataset were calculated for the demographic, clinical, anatomic, VF and corneal biomechanical parameters. Comparisons were made between groups. Receiver operating characteristic (ROC) analyses were performed to find an appropriate cut-off (defined as the point nearest to the upper left corner of the ROC curve) and to determine the area under the curve (AUROC) of each DCR variable for the presence of glaucoma among highly myopic and non-myopic eyes.

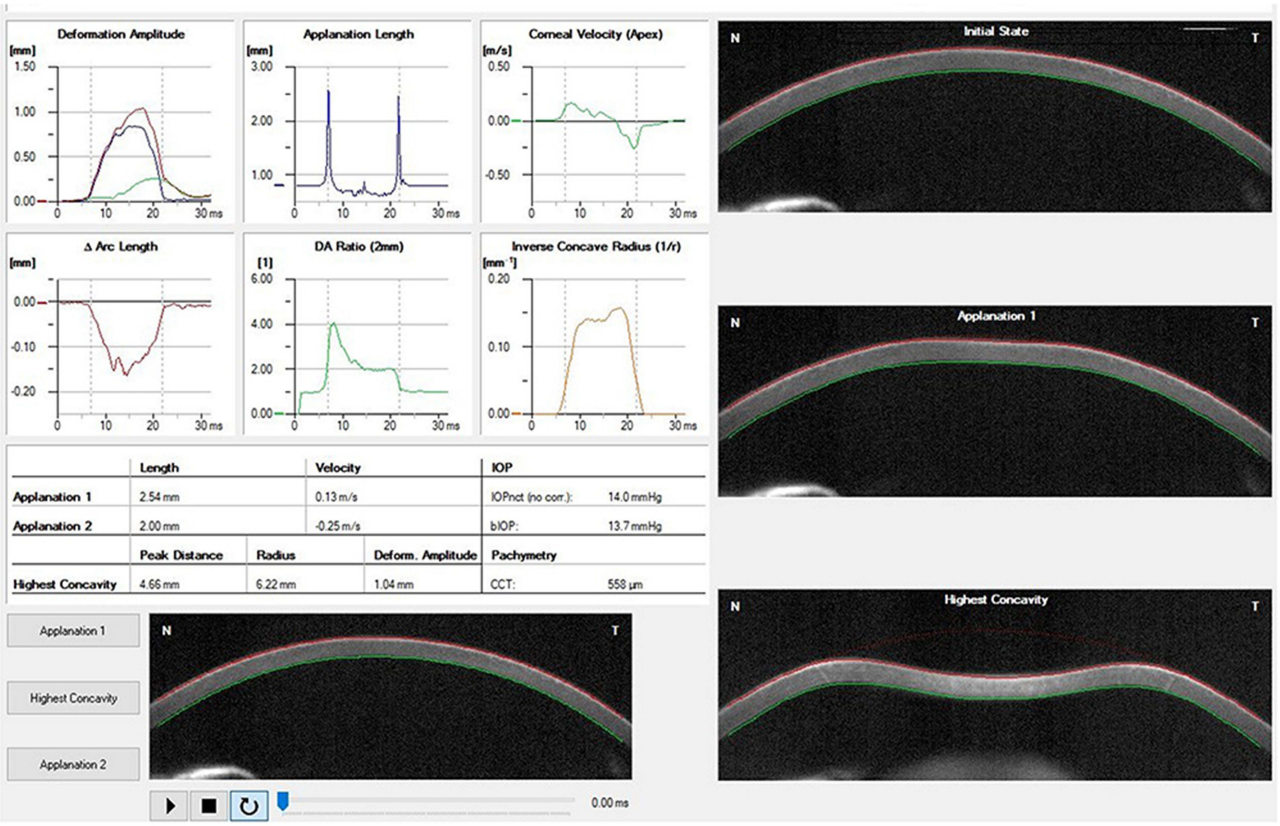

Figure 1 Corvis ST® – Dynamic Corneal Response Layout.

A logistic regression was performed to assess the effect of corneal biomechanics in glaucoma for 1) eyes with high myopia (HMG and HMNG), 2) non-myopic eyes (POAG and NMNG), and 3) all study population. Candidate predictors in multivariable analyses were the biomechanical variables retrieved from OCULUS Corvis® ST. Variables were screened to identify associations with glaucoma at the $p < 0.25$ level. Predictors meeting this condition were included in stepwise backward elimination analysis in which $p < 0.05$ served as the criterion for retention into the full model. For the model, including all study populations, interaction terms were tested with the adjustment of biomechanical parameters that were differentially included in the two previous models for the presence of high myopia. All analyses were performed using the SPSS® and Stata® software. All values are shown as mean ± standard deviation unless otherwise specified. All p-values (p) were 2-sided, and p-values < 0.05 were considered significant.

Results

A stepwise analysis through 5 steps was carried out in the present study.

The first step was comparing HMG and HMNG and POAG and NMNG groups regarding age, gender, AL, MRSE, GAT-IOP, and IOP lowering drops (Table 2). The HMG group was older than the HMNG group, and the POAG group was older than the NMNG group ($p < 0.001$). HMG eyes had higher AL ($p < 0.001$) and GAT-IOP ($p = 0.017$) mean values than the HMNG ones. Myopic eye groups had no differences in MRSE ($p = 0.690$), but within the non-myopic eye groups, the NMNG eyes were more hyperopic than the POAG ones ($p = 0.027$).

The second step was comparing the two groups of glaucomatous eyes (HMG and POAG) (Table 3). The average number of IOP lowering drops was similar in the two groups ($p = 0.230$). All ppRNFL average values were inferior in the HMG ($p < 0.05$ in all). POAG eyes showed higher PSD ($p = 0.04$), but none of the other VF parameters showed significant differences between these two groups ($p > 0.05$ in all).

Table 1 Scheimpflug Camera-Derived Corneal Biomechanical Parameters with Explanation

Parameters	Abbreviations	Explanation
cIOP [mmHg]	**cIOP**	Corvis-derived intraocular pressure
cCCT [µm]	**cCCT**	Corvis-derivated central corneal thickness
1st generation parameters		**Description**
Deformation Amp. Max [mm]	**MaxDefoA**	Corneal deformation amplitude during MaxDT, as the sum of corneal deflection amplitude and MaxWEM
A1 Time [ms]	**A1T**	Time from the measurement beginning to the first applanation moment
A1 Velocity [m/s]	**A1V**	Velocity of the corneal apex during the first applanation
A2 Time [ms]	**A2T**	Time from the measurement beginning to the second applanation moment
A2 Velocity [m/s]	**A2V**	Velocity of the corneal apex during the second applanation
HC Time [ms]	**HCT**	Time from the measurement beginning to the moment of reaching the highest concavity (HC)
Peak Dist. [mm]	**HCPD**	Distance between the corneal peaks at the HC
Radius [mm]	**HCR**	Radius of corneal curvature during the HC
A1 Deformation Amp. [mm]	**A1DefoA**	Corneal deformation amplitude during A1, as the sum of corneal deflection amplitude and MaxWEM
HC Deformation Amp. [mm]	**HCDefoA**	Corneal deformation amplitude during HC, as the sum of corneal deflection amplitude and MaxWEM
A2 Deformation Amp. [mm]	**A2DefoA**	Corneal deformation amplitude during A2, as the sum of corneal deflection amplitude and MaxWEM
A1 Deflection Length [mm]	**A1DL**	Horizontal length of the flattened cornea at the A1
HC Deflection Length [mm]	**HCDL**	Horizontal length of the flattened cornea at the HC
A2 Deflection Length [mm]	**A2DL**	Horizontal length of the flattened cornea at the A2
A1 Deflection Amp. [mm]	**A1DA**	Corneal deflection amplitude during A1, determined as the displacement of the corneal apex in relation to the initial state without the MaxWEM quantification
HC Deflection Amp. [mm]	**HCDA**	Corneal deflection amplitude during HC, determined as the displacement of the corneal apex in relation to the initial state without the MaxWEM quantification
A2 Deflection Amp. [mm]	**A2DA**	Corneal deflection amplitude during A2, determined as the displacement of the corneal apex in relation to the initial state without the MaxWEM quantification
Deflection Amp. Max [mm]	**MaxDA**	Corneal deformation amplitude during MaxDT, as the sum of corneal deflection amplitude and MaxWEM
Deflection Amp. Max [ms]	**MaxDT**	Moment of the maximum deformation, during the oscillatory phase near HC
Whole Eye Movement Max [mm]	**MaxWEM**	Amplitude of the Maximum whole eye movement
Whole Eye Movement Max [ms]	**MaxWEMT**	Time at which occurs the amplitude of the Maximum whole eye movement (near A2)

(*Continued*)

https://doi.org/10.2147/OPTH.S426635 DovePress

Table 1 (Continued).

Parameters	Abbreviations	Explanation
A1 Deflection Area [mm²]	**A1DArea**	Deflection area in A1
HC Deflection Area [mm²]	**HCDArea**	Deflection area in HC
A2 Deflection Area [mm²]	**A2DArea**	Deflection area in A2
A1 dArc Length [mm]	**A1dArcL**	Delta arc length of corneal surface in A1
HC dArc Length [mm]	**HCdArcL**	Delta arc length of corneal surface in HC
A2 dArc Length [mm]	**A2dArcL**	Delta arc length of corneal surface in A2
dArcLengthMax [mm]	**MaxdArcL**	Delta arc length of corneal surface in MaxDT
2nd generation parameters		**Description**
Max InverseRadius [mm^-1]	**MIR**	1 / HCR
DA Ratio Max (2mm)	**DARM2**	Ápex MaxDA / MaxDA at 2mm from the ápex
PachySlope [µm]	**PqS**	Peripheric (8mm horizontal) pachymetry / Ápex pachymetry
DA Ratio Max (1mm)	**DARM1**	Ápex MaxDA / MaxDA at 1mm from the ápex
Ambrosio Relational Thickness (8mm)	**ARTh**	Ambrosio Relational Thickness within the horizontal 8mm cornea of the image
Biomechanically-corrected IOP	**bIOP**	IOP adjusted for biomechanical parameters
Integrated Radius [mm^-1]	**IR**	Area under the curve of the 1/HCR function
Stiffness parameter in A1	**SP-A1**	Air puff pressure - bIOP / A1DA
Corvis biomechanical index	**CBI**	Exponential function score made through a logistic regression analysis of 6 parameters (SP-A1, DARM1, DARM2, ARTh, A1V and MaxDefoA) and adjusted for IOP and CCT to describe ectasia risk
Stress Strain Index	**SS-I**	Finite element modeling algorithm for the estimation of the non-linear in vivo biomechanical behaviour in corneal with normal topography

https://doi.org/10.2147/OPTH.S426635 DovePress

Table 2 Descriptive Statistics, General and Within the Four Groups

	All Sample		HMG		HMNG		p-Value	POAG		NMNG		p-Value
	Mean	SD	Mean	SD	Mean	SD		Mean	SD	Mean	SD	
Age	59.3	16.8	62.9	12.4	38.8	9.7	**<0.001**	73.8	11.3	62.6	10.2	**<0.001**
AL	27.74	3.8	30.32	3.6	26.79	1.5	**<0.001**					
MRSE	-2.96	6.2	-9.45	5.6	-10.02	4.4	0.690	0.97	1.2	1.57	1.5	**0.027**
GAT-IOP	14.4	3.1	15.7	3.9	14.2	1.8	**0.017**	13.7	3.1	13.8	2.6	0.832
Gender within group	M 97 (46.2%) / F 112 (53.3%)		M 45.3% / F 54.7%		M 49.1% / F 50.9%			M 46.0% / F 54.0%		M 45.3% / F 54.7%		0.976*

Notes: *Chi-squared test. Bold text: statistical significance for a p<0.05.
Abbreviations: AL, axial length; MRSE, manifest refraction spherical equivalent; GAT-IOP, pachymetry-adjusted Goldmann applanation tonometry-intraocular pressure; HMG, high myopia with glaucoma; HMNG, High myopia without glaucoma; POAG, primary open-angle glaucoma; NMNG, non-myopia and non-glaucoma; M; masculine; F, Feminine.

Table 3 Descriptive Statistics, Comparison Between the Glaucomatous Groups

	HMG		POAG		p-value
	Mean	SD	Mean	SD	
Number of Topical medications	2.13	1.1	1.88	1.0	0.230
SD-OCT					
Inaccurate/impossible segmentation (n/%)	33/62.3%		0/0%		**<0.001***
ppRNFLT M	47.68	27.7	67.90	19.8	**<0.001**
ppRNFLT IT	60.06	47.4	86.94	39.0	**0.003**
ppRNFLT SN	43.08	32.9	77.66	28.4	**<0.001**
ppRNFLT ST	51.85	41.6	84.34	31.4	**<0.001**
ppRNFLT N	41.30	28.6	56.90	18.4	**0.003**
ppRNFLT T	43.91	25.9	55.40	16.7	**0.011**
VFI					
GHT outside normal limits within group (n/%)	35/74.5%		39/83%		0.319*
VFI (%)	75.41	24.1	72.80	23.2	0.603
MD	−11.70	7.7	−11.37	6.3	0.823
PSD	6.64	3.3	8.15	3.7	**0.040**

Notes: *Chi-squared test. Bold text: statistical significance for a p<0.05.
Abbreviations: HMG, high myopia with glaucoma; HMNG, High myopia without glaucoma; POAG, primary open-angle glaucoma; SD-OCT, spectral domain optical coherence tomography; ppRNFLT, peripapillary retinal nerve fiber layer thickness (μm); M, mean; IT, inferior-temporal; SN, superior-nasal; ST, superior-temporal; N, nasal; T, temporal; VF, visual field; GHT, Glaucoma hemifield test; VFI, visual field index; MD, mean deviation; PSD, pattern standard deviation.

The third step was a comparison of the Scheimpflug-derived biomechanical parameters between two pairs of groups: pair 1, HMG, and HMNG and pair 2, POAG, and NMNG (Tables 4 and 5). In the first place, HMG showed only a trend to low cCCT values compared with HMNG eyes (pair 1, $p = 0.055$), while POAG showed inferior cCCT than NMNG eyes (pair 2, $p < 0.001$). Within the pair 1 comparative analysis, HMG eyes showed superior A2DL, CBI and SS-I and inferior A1V and A2T ($p < 0.05$ in all). Within pair 2, POAG eyes showed inferior A2DefoA, A1DL, A2DL and A1DArea ($p < 0.05$ in all), superior values in the MIR and DARM1 ($p < 0.05$), and a trend to superior DARM2 ($p = 0.051$) and CBI ($p = 0.053$). On the other hand, both the Corvis-derived IOP (cIOP) and bIOP showed no significant differences between groups within each pair ($p > 0.005$ in all).

The fourth step was a calculation of the receiver operating curves (ROC) including area under the curve (AUROC) and best cut-off points to discriminate these pairs of groups through the Scheimpflug-derived biomechanical parameters,

https://doi.org/10.2147/OPTH.S426635 DovePress

Table 4 All Receiver Operating Curves (ROC) for Biomechanical Parameters, Including Area Under Curve (AUROC) and Best Cut-off Points to Discriminate Groups, Pair 1: HMG (High Myopia with Glaucoma) and HMNG (High Myopia Without Glaucoma)

Biomechanical parameter	Abbreviation	HMG (n=53)	HMNG (n=53)	P–Value	AUROC	95% CI	Cut–off	Sensitivity	Specificity
cIOP [mmHg]	**cIOP**	16.91±5.69	15.97±1.94	0.26	47.35%	35.95–58–74%	16.75	36%	74%
cCCT [µm]	**cCCT**	535.13±43.99	550.83±38.68	0.055	39.15%	28.13–50.17%	565.5	28%	67%
1st generation parameters									
Deformation Amp. Max [mm]	**MaxDefoA**	1.08±0.21	1.04±0.10	0.25	**62.14%**	51.12–73.16%	**1.09**	**57%**	**72%**
A1 Time [ms]	**A1T**	7.99±0.81	7.85±0.26	0.21	47.19%	35.79–58.58%	7.94	36%	74%
A1 Velocity [m/s]	**A1V**	0.13±0.02	0.13±0.02	**0.043**	40.49%	29.62–51.37%	0.13	51%	43%
A2 Time [ms]	**A2T**	21.28±0.86	21.70±0.35	**0.001**	33.34%	22.94–43.74%	21.54	42%	40%
A2 Velocity [m/s]	**A2V**	–0.28±0.11	–0.29±0.04	0.67	41.60%	30.48–52.72%	0.28	38%	60%
HC Time [ms]	**HCT**	17.26±0.834	17.44±0.56	0.20	44.45%	33.50–55.39%	17.44	40%	53%
Peak Dist. [mm]	**HCPD**	4.99±0.63	4.98±0.30	0.87	59.18%	47.99–70.37%	5.01	65%	57%
Radius [mm]	**HCR**	6.47±0.96	6.35±0.62	0.42	54.75%	43.70–65.80%			
A1 Deformation Amp. [mm]	**A1DefoA**	0.14±0.012	0.14±0.01	0.35	55.52%	44.25–66.79%	0.14	47%	66%
HC Deformation Amp. [mm]	**HCDefoA**	1.08±0.21	1.04±0.10	0.25	**62.14%**	51.12–73.16%	**1.09**	**57%**	**72%**
A2 Deformation Amp. [mm]	**A2DefoA**	0.33±0.11	0.32±0.04	0.42	50.80%	39.25–62.36%	0.34	47%	70%
A1 Deflection Length [mm]	**A1DL**	2.29±0.22	2.27±0.18	0.66	54.92%	43.74–66.10%	2.27	52%	60%
HC Deflection Length [mm]	**HCDL**	6.53±0.88	6.45±0.56	0.57	58.44%	47.23–69.64%	6.85	46%	81%
A2 Deflection Length [mm]	**A2DL**	3.16±1.11	2.68±0.73	**0.010**	**61.80%**	50.99–72.61%	**2.76**	**55%**	**62%**
A1 Deflection Amp. [mm]	**A1DA**	0.09±0.01	0.09±0.02	0.40	56.92%	51.21–73.33%	0.09	47%	70%
HC Deflection Amp. [mm]	**HCDA**	0.94±0.23	0.88±0.18	0.18	**62.26%**	46.00–68.28%	**0.99**	**55%**	**75%**
A2 Deflection Amp. [mm]	**A2DA**	0.10±0.08	0.10±0.05	0.99	57.14	46.00–68.28%	0.10	62%	57%
Deflection Amp. Max [mm]	**MaxDA**	0.98±0.29	0.89±0.17	0.071	**63.15%**	52.23–74.07%	**0.99**	**55%**	**75%**
Deflection Amp. Max [ms]	**MaxDT**	16.63±1.95	16.31±2.32	0.44	46.42%	35.29–57.55%	16.37	57%	47%
Whole Eye Movement Max [mm]	**MaxWEM**	0.23±0.08	0.22±0.04	0.38	51.07%	39.62–62.51%	0.25	42%	77%

Whole Eye Movement Max [ms]	**MaxWEMT**	21.52±1.11	21.47±0.56	0.78	56.34%	45.07–67.60%	21.76	45%	77%
A1 Deflection Area [mm²]	**A1DArea**	0.17±0.04	0.18±0.07	0.42	50.98%	39.79–62.16%	0.17	53%	58%
HC Deflection Area [mm²]	**HCDArea**	3.41±1.07	3.22±0.58	0.26	**60.98%**	49.86–72.10%	**3.72**	**49%**	**79%**
A2 Deflection Area [mm²]	**A2DArea**	0.14±0.55	0.23±0.05	0.27	57.32%	46.25–68.38%	0.23	55%	66%
A1 dArc Length [mm]	**A1dArcL**	–0.02±0.004	–0.02±0.004	0.60	43.00%	32.00–54.01	0.02	36%	62%
HC dArc Length [mm]	**HCdArcL**	–0.12±0.08	–0.12±0.02	0.82	45.69%	34.38–57.00%	0.11	43%	62%
A2 dArc Length [mm]	**A2dArcL**	0.01±0.19	–0.02±0.01	0.20	44.05%	32.96–55.15%	0.02	58%	38%
dArcLengthMax [mm]	**MaxdArcL**	–0.15±0.04	–0.13±0.03	0.052	39.80%	28.79–50.81%	0.12	32%	66%
2nd generation parameters									
Max InverseRadius [mm^–1]	**MIR**	0.20±0.07	0.19±0.01	0.34	46.56%	35.34–57.79%	0.19	40%	58%
DA Ratio Max (2mm)	**DARM2**	3.97±0.71	4.06±0.40	0.43	50.44%	39.24–61.63%	4.02	58%	48%
PachySlope [µm]	**PqS**	21.42±130.74	39.53±12.24	0.32	37.08%	25.82–48.34%	44.99	26%	83%
DA Ratio Max (1mm)	**DARM1**	1.65±0.91	1.51±0.12	0.28	50.75%	39.63–61.85%	1.51	62%	43%
Ambrosio Relational Thickness (horizontal 8mm)	**ARTh**	752.00±653.12	640.15±160.30	0.23	46.00%	34.44–57.56%	705.57	33%	77%
Biomechanically corrected IOP	**bIOP**	15.69±5.09	15.25±1.81	0.56	43.40%	31.82–54.97%	16.9	32%	83%
Integrated Radius [mm^–1]	**IR**	8.845±3.49	8.94±1.02	0.85	42.22%	31.31–53.34%	8.89	45%	51%
Stiffness parameter in A1	**SP–A1**	119.18±25.72	114.20±15.54	0.23	55.08%	43.91–66.25%	120.55	47%	71%
Corvis biomechanical index	**CBI**	0.31±0.31	0.19±0.18	**0.020**	55.73%	43.55–67.91%	0.23	51%	73%
Stress Strain Index	**SS–I**	1.10±0.52	0.92±0.22	**0.022**	56.23%	44.82–67.64%	1.017	47%	70%

Note: Bold text: statistical significance for a p<0.05.
Abbreviations: HMG, high myopia with glaucoma; HMNG, High myopia without glaucoma; AUROC, Area under the receiver operating characteristic curve.

https://doi.org/10.2147/OPTH.S426635 DovePress

https://doi.org/10.2147/OPTH.S426635 DovePress

Table 5 All Receiver Operating Curves (ROC) for Biomechanical Parameters, Including Area Under Curve (AUROC) and Best Cut-off Points to Discriminate Groups, Pair 2: POAG (Primary Open-Angle Glaucoma) and NMNG (Non-Myopia and Non-Glaucoma)

Biomechanical parameter	Abbreviation	POAG (n=50)	NMNG (n=53)	P-value	AUROC	95% CI	Cut-off	Sensitivity	Specificity
cIOP [mmHg]	cIOP	15.47±5.36	15.23±2.82	**0.77**	40.94%	29.70–52.18%	14.75	44%	43%
cCCT [µm]	cCCT	529.48±36.49	560.55±33.66	**<0.001**	26.21%	16.63–35.79%	532.5	52%	23%
1st generation parameters									
Deformation Amp. Max [mm]	MaxDefoA	1.02±0.17	1.01±0.10	**0.92**	53.13%	41.37–64.89%	1.08	44%	81%
A1 Time [ms]	A1T	7.81±0.75	7.75±0.36	**0.64**	40.92%	29.65–52.20%	7.68	46%	43%
A1 Velocity [m/s]	A1V	0.14±0.02	0.14±0.019	**0.73**	53.45%	42.10–64.81%	0.14	50%	68%
A2 Time [ms]	A2T	21.73±0.67	21.95±0.46	**0.055**	39.92%	28.83–51.02%	21.91	44%	49%
A2 Velocity [m/s]	A2V	−0.25±0.05	−0.24±0.04	**0.71**	42.75%	31.39–54.12%	−2.445	34%	62%
HC Time [ms]	HCT	17.63±0.59	17.79±0.63	**0.18**	41.77%	30.81–52.73%	17.90	30%	62%
Peak Dist. [mm]	HCPD	4.76±0.53	4.72±0.31	**0.64**	57.28%	45.82–68.75%	4.77	66%	60%
Radius [mm]	HCR	6.60±0.89	6.99±1.30	**0.080**	38.75%	27.74–49.77%	6.50	58%	42%
A1 Deformation Amp. [mm]	A1DefoA	0.14±0.013	0.14±0.01	**0.82**	46.49%	35.05–57.93%	0.14	40%	62%
HC Deformation Amp. [mm]	HCDefoA	1.02±0.17	1.01±0.10	**0.92**	53.13%	41.37–64.89%	1.08	44%	81%
A2 Deformation Amp. [mm]	A2DefoA	0.39±0.09	0.42±0.07	**0.031**	35.53%	24.44–46.50%	0.45	22%	79%
A1 Deflection Length [mm]	A1DL	2.28±0.15	2.35±0.12	**0.010**	33.45%	22.85–44.05%	2.34	32%	49%
HC Deflection Length [mm]	HCDL	6.14±0.77	6.11±0.44	**0.80**	52.34%	40.86–63.82%	6.04	64%	47%
A2 Deflection Length [mm]	A2DL	2.84±0.66	3.22±0.61	**0.003**	32.08%	21.54–42.61%	3.44	22%	66%
A1 Deflection Amp. [mm]	A1DA	0.09±0.01	0.097±0.01	**0.10**	39.32%	28.03–50.61%	0.097	36%	53%
HC Deflection Amp. [mm]	HCDA	0.84±0.16	0.81±0.13	**0.26**	59.19%	47.76–70.62%	0.86	56%	70%
A2 Deflection Amp. [mm]	A2DA	0.11±0.01	0.11±0.05	**0.73**	29.89%	19.55–40.22%	0.10	66%	17%
Deflection Amp. Max [mm]	MaxDA	0.86±0.16	0.85±0.12	**0.74**	58.30%	46.73–69.87%	0.89	56%	74%
Deflection Amp. Max [ms]	MaxDT	16.44±0.88	16.59±1.74	**0.59**	51.96%	40.63–63.30%	16.64	46%	62%
Whole Eye Movement Max [mm]	MaxWEM	0.29±0.08	0.33±0.14	**0.15**	38.83%	27.69–49.97%	0.34	22%	79%

Whole Eye Movement Max [ms]	MaxWEMT	22.09±0.85	22.10±1.13	**0.93**	51.92%	40.34–63.50%	22.02	60%	51%
A1 Deflection Area [mm²]	A1DArea	0.17±0.02	0.18±0.02	**0.004**	33.81%	23.22–44.40%	0.18	34%	49%
HC Deflection Area [mm²]	HCDArea	2.91±0.77	2.78±0.53	**0.32**	57.66%	46.19–69.13%	2.95	58%	68%
A2 Deflection Area [mm²]	A2DArea	0.24±0.06	0.24±0.27	**0.95**	30.08%	19.68–40.47%	0.3	14%	77%
A1 dArc Length [mm]	A1dArcL	−0.02±0.004	−0.02±0.002	**0.15**	62.55%	51.59–73.51%	−0.02	52%	68%
HC dArc Length [mm]	HCdArcL	−0.12±0.03	−0.12±0.03	**0.70**	58.09%	46.68–69.51%	−0.12	60%	60%
A2 dArc Length [mm]	A2dArcL	−0.02±0.01	−0.01±0.11	**0.49**	70.26%	59.73–80.80%	−0.03	72%	66%
dArcLengthMax [mm]	MaxdArcL	−0.20±0.42	−0.17±0.17	**0.59**	52.11%	40.46–63.76%	−0.14	46%	68%
2nd generation parameters									
Max InverseRadius [mm^-1]	MIR	0.19±0.02	0.18±0.02	**0.049**	61.45%	50.53–72.38%	0.19	44%	79%
DA Ratio Max (2mm)	DARM2	4.26±0.49	4.07±0.46	**0.051**	62.68%	51.72–73.64%	4.14	68%	57%
PachySlope [µm]	PqS	32.38±14.75	34.40±10.27	**0.42**	39.58%	28.54–50.63%	34.03	46%	47%
DA Ratio Max (1mm)	DARM1	1.55±0.05	1.53±0.05	**0.006**	65.89%	55.29–76.49%	1.53	74%	57%
Ambrosio Relational Thickness (horizontal 8mm)	ARTh	621.27±213.11	652.52±178.77	**0.42**	45.74%	34.22–57.26%	684.52	42%	68%
Biomechanically-corrected IOP	bIOP	14.15±5.13	13.51±2.32	**0.42**	46.51%	34.97–58.05%	14.25	36%	70%
Integrated Radius [mm^-1]	IR	8.81±1.53	8.56±1.04	**0.33**	59.13%	47.74–70.53%	9.24	46%	79%
Stiffness parameter in A1	SP-A1	112.07±19.92	116.31±20.71	**0.29**	42.75%	31.58–53.92%	107.57	64%	34%
Corvis biomechanical index	CBI	0.29±0.30	0.18±0.24	**0.053**	60.78%	49.65–71.92%	0.08	68%	55%
Stress Strain Index	SS-I	1.37±0.23	1.29±0.18	**0.058**	59.65%	48.56–70.75%	1.31	54%	56%

Note: Bold text: statistical significance for a p<0.05.
Abbreviations: POAG, primary open-angle glaucoma; NMNG, non-myopia and non-glaucoma; AUROC, Area under the receiver operating characteristic curve.

https://doi.org/10.2147/OPTH.S426635

respectively (Tables 4 and 5). None AUROC of a single parameter was found to be above 0.8 but AUROC's above 0.6 were found in 6 parameters applied to discriminate between HMG and HMNG eyes (DefAmpMax; HCDefoA, A2DL, HCDA, MaxDA, HCDArea) (Figure 2) and 6 parameters to discriminate between POAG and NMNG eyes (A1dArcL, A2dArcL, MIR, DARM1, DARM2 and CBI) (Figure 3).

The fifth step comprised the construction of multivariable regression models to determine potential associations between biomechanical variables and the presence of glaucoma (Figures 4–6). For eyes with high myopia, the model with the highest power of prediction for the presence of glaucoma included five parameters (A1T, MaxDA, MaxdArcL, SP-A1 and SSI) with an AUROC of 0.947. For non-myopic eyes, the model with the highest power of prediction for the presence of glaucoma included six parameters (A2T, HCT, HCR, A1DArea, DARM2, SS-I) with an AUROC of 0.857. In the final model, including all of the 209 eyes and adjusted for the presence of high myopia, the highest power of prediction for the existence of glaucoma included eight biomechanical parameters (A1T, A2T, MaxDA, A1DArea, HCDArea, MIR, DARM1, SS-I) with an AUROC of 0.917.

Discussion

Recent studies with Corvis reported[23] alteration in corneal biomechanics with age, but there is still controversy in literature.[23–25] In the present study, patients with glaucoma are older than patients without glaucoma and, within the glaucomatous ones, POAG patients are older than those with HMG. As glaucoma is a progressive disease, it will always be difficult to make a complete age-matched comparison in this setting. However, theoretically, it is generally believed that age has a stiffer effect on corneal tissue due to a natural crosslinking effect. Thus, this highlights the differences in a softer behavior found in both groups of glaucomatous eyes in the present study.

In the IOP assessment setting, the pattern of average values in each group was similar between GAT-IOP, cIOP, and bIOP. However, besides the higher GAT-IOP observed in the HMG group, the lack of significant differences in Corvis-derived values highlights the capability of this technology in overcoming both practical difficulties of the applanation-derived assessment and the handicaps associated with the empiric Imbert Fick principle implicit in GAT-IOP, particularly in eyes with different anatomy like in high myopia. In fact, in 2016, Elsheikh et al[18] started to build a model based on finite element analysis reducing the reliance of IOP measurements on corneal thickness and age and then, in 2018, after the studies of Vinciguerra group, the bIOP was proven to be the most accurate non-invasive corneal-dissociated IOP assessment.[19,20]

The importance given to IOP is more related with the fact that it is the only proven modifiable risk factor for glaucomatous damage progression rather than a linear pathophysiologic association to damage itself. In fact, within the mechanical hypothesis of glaucoma, the paradigm of the optic nerve head as part of a biomechanical structure encompassing LC, scleral canal wall, and peripapillary sclera has gained consistency and, thus, modeling the ONH as a biomechanical structure generates a group of testable hypotheses regarding the central mechanisms of axonal compromise due to mechanical failure of the aforementioned structures and provides a logic for classifying the principal components of the susceptibility of an individual ONH to a given level of IOP.[10]

The triangle encompassing the anatomy of peripapillary sclera and, mainly, LC (thinned[15,26,] with defects[27] or posteriorly displaced[28]), increased AL and glaucomatous damage is well described. Still, the precise quantification of the interrelationship between the three vertices remains challenging. Nevertheless, the biomechanical behavior associated with a given ONH can be more critical than its anatomy. As the Scheimpflug technology increased the complexity of corneal biomechanics evaluation compared to the former ones,[29] there is still a lack of data regarding the differential role of the various Corvis-derived DCRs in the glaucoma spectrum. In the setting of high myopia, there is some evidence that corneal biomechanical properties are related to axial length,[30,31] but, again, if the anatomy vertice is replaced by biomechanical behavior, the challenge remains. Nevertheless, the novel 2nd generation parameters and the bIOP are suggested nowadays as a new risk factor for the development of NTG[32,33] and functional progression in POAG.[33] However, the evidence is still poor, and there is a lack of data within the high myopia subset.

The Scheimpflug-camera-derived basic analysis describes corneal biomechanical behavior in three major timepoints: applanation 1 (A1), highest concavity (HC) and applanation 2 (A2). Additionally, it gives information from the maximum deformation on the oscillatory phase (MaxDT) and from Whole Eye Movement (WEM), all within the nearly 35

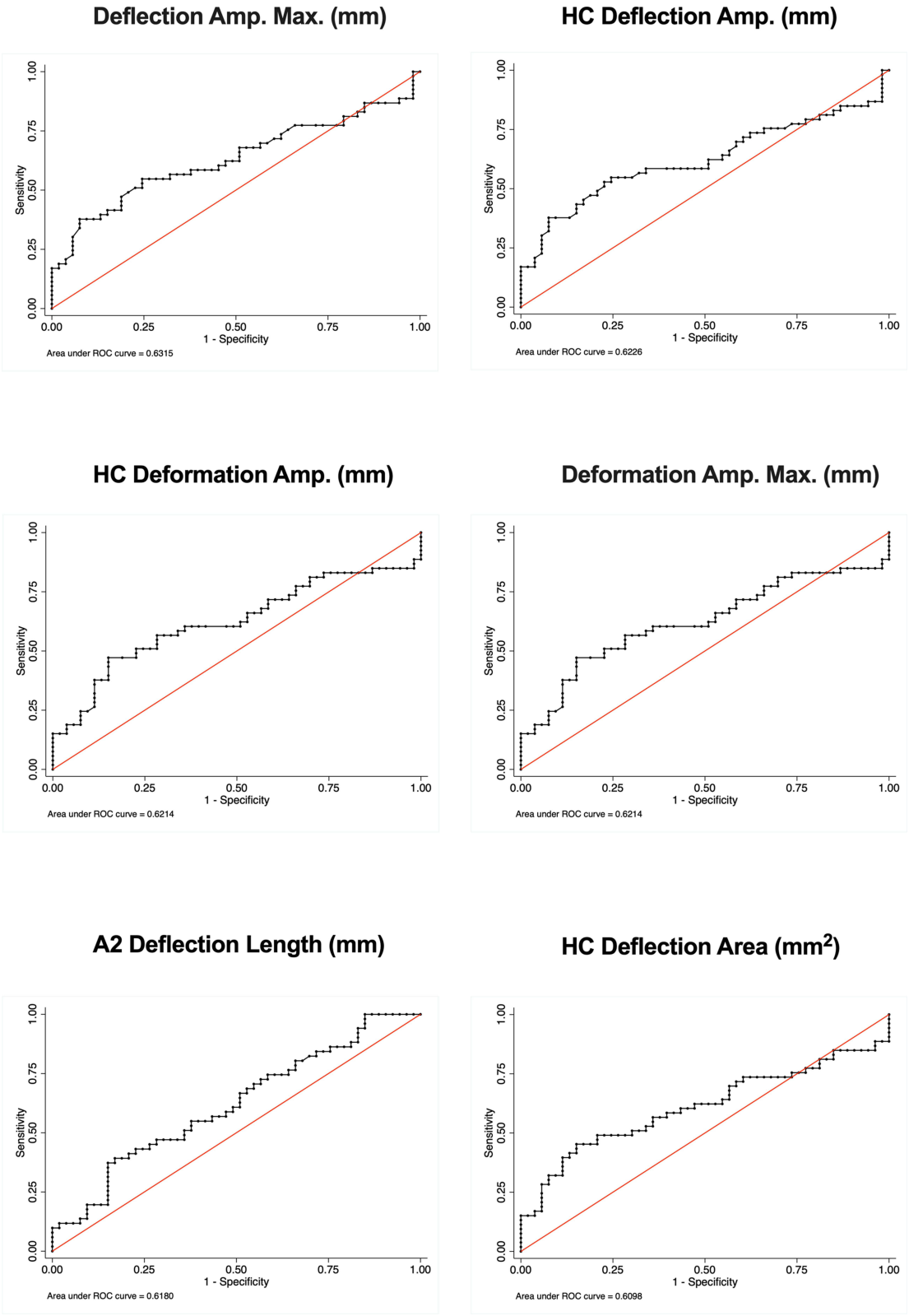

Figure 2 Best receiver operating curves (ROC) for biomechanical parameters, including area under curve (AUROOC) to discriminate groups (pair 1): HMG (high myopia with glaucoma) and HMNG (High myopia without glaucoma).

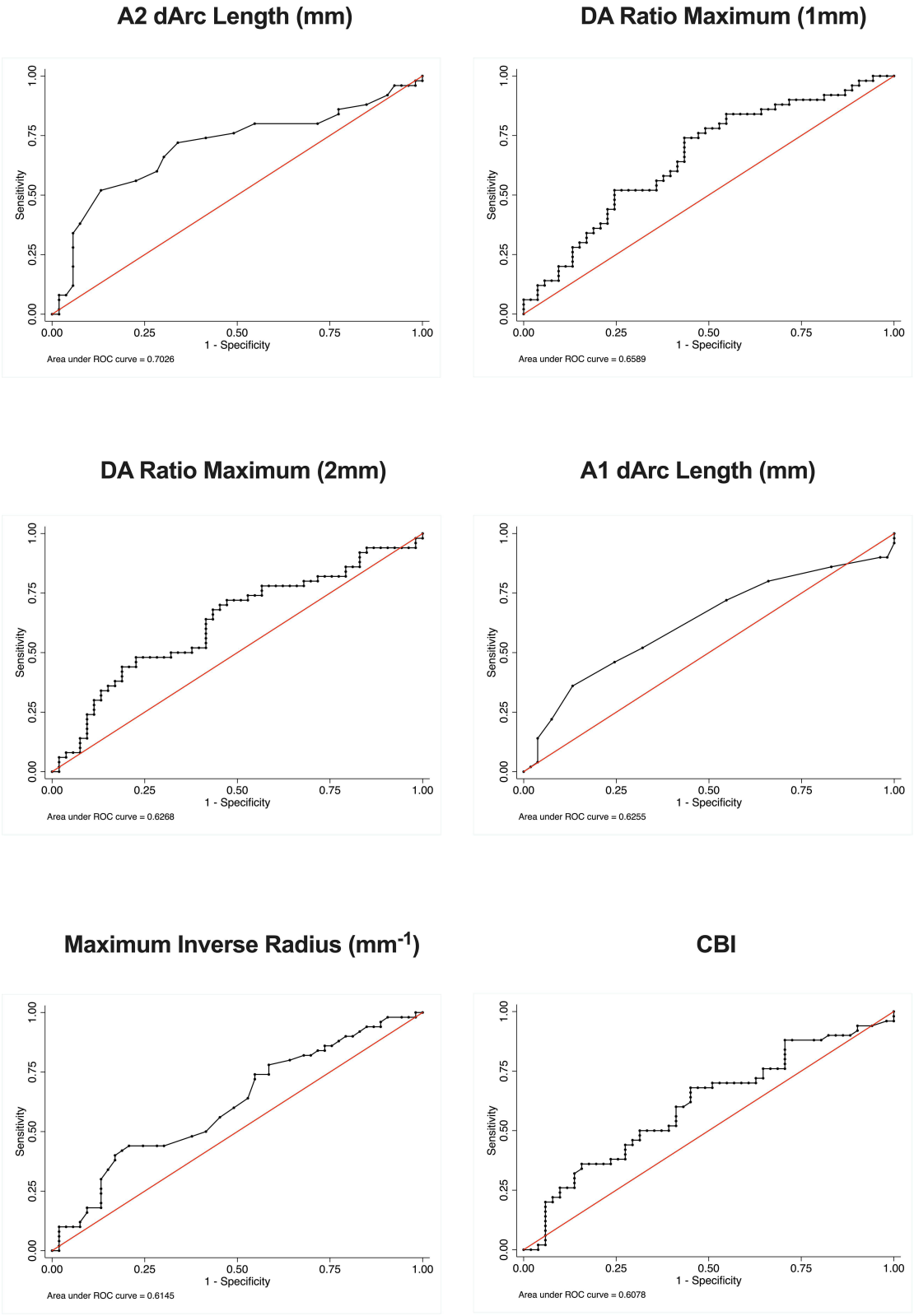

Figure 3 Best receiver operating curves (ROC) for biomechanical parameters, including area under curve (AUROOC) to discriminate groups (pair 2): POAG (primary open-angle glaucoma) and NMNG (non-myopia and non-glaucoma).

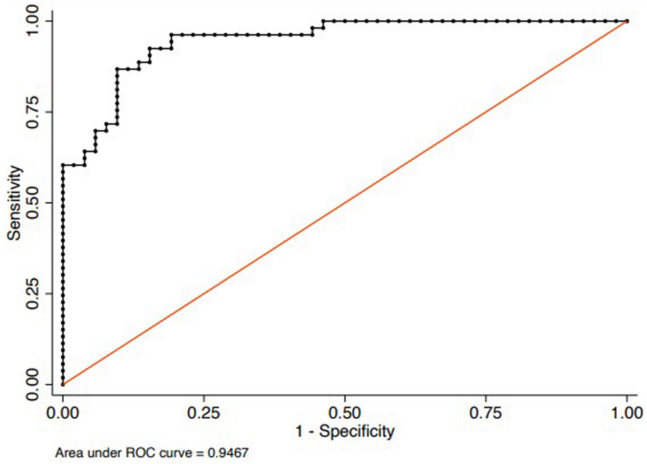

Figure 4 Receiver operating curve (ROC) including area under curve (AUROC) for the biomechanical multivariable logistic regression model with the highest power of prediction for the presence of glaucoma in eyes with high myopia (pair 1): HMG (high myopia with glaucoma) and HMNG (high myopia without glaucoma).

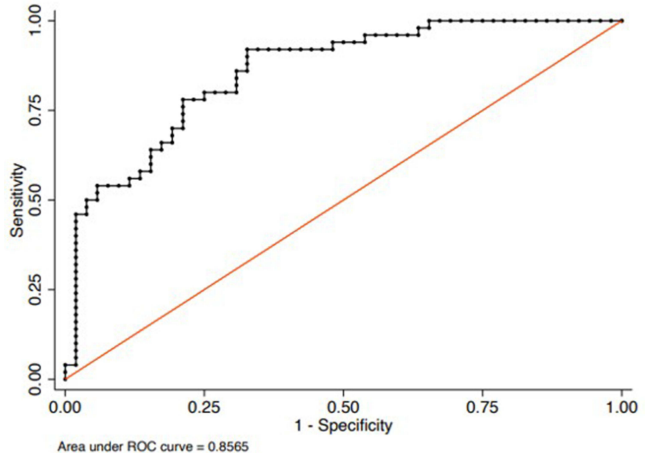

Figure 5 Receiver operating curve (ROC) including area under curve (AUROC) for the biomechanical multivariable logistic regression model with the highest power of prediction for the presence of glaucoma in eyes with high myopia (pair 2): POAG (primary open-angle glaucoma) and NMNG (non-myopia and non-glaucoma).

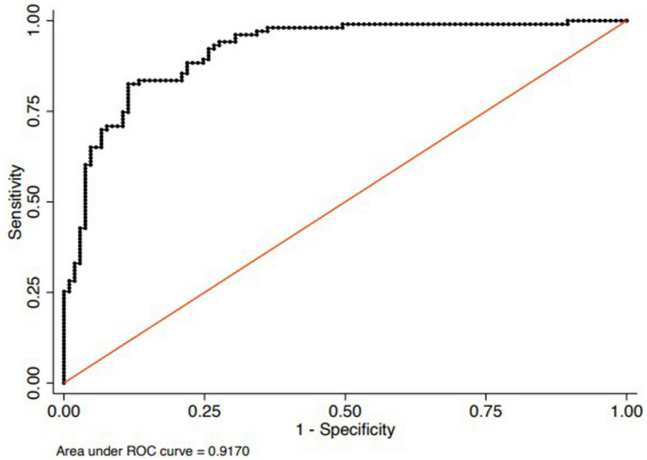

Figure 6 Receiver operating curve (ROC) including area under curve (AUROC) for the final biomechanical multivariable logistic regression model with the highest power of prediction for the presence of glaucoma in all eyes, adjusted for the presence of high myopia.

milliseconds interval in which the cornea makes the ingoing and outgoing movements after the air puff.[34] Additionally, to known lower CCT, theoretically, it is expected that eyes with less stiffness were associated to higher values on the deformation and deflection amplitudes, deflection areas and applanation lengths in all timepoints, lower A1T with higher A1V but higher A2T with lower A2V, lower MaxDT and higher peak distance (HCPD) and lower radius (HCR) when the cornea is in the Highest Concavity timepoint (HCT).[35,36] Within the setting of a single-parameter analysis, the A1T, A2T, and HC-related parameters were the first described as the most important. On the other hand, deflection areas were thought to be less important parameters within this basic analysis.[35,36] Besides the comprehensive limitations of single parameters to describe the complex biomechanical behavior, they are affected by IOP (otherwise none of the air-puff tonometers would work). Nevertheless, the large amount of data from all these parameters mentioned above began to be studied through various methods towards the construction of models of characterization of increasing consistency, and 2nd generation parameters are in constant evolution nowadays.[35] The stiffness parameter A1 (SP-A1), created by the group of Roberts et al,[37] was defended as the most accurate in defining the global eye rigidity, including the relation of IOP with both corneal and scleral biomechanical components. Moreover, the CBI was built by Vinciguerra et al[38] as an exponential function score made through a logistic regression analysis of 6 DCR parameters and adjusted for IOP and CCT and is defended as the most embracing corneal biomechanical descriptor in the ectasia setting. Nevertheless, even more recent is the Stress-Strain Index (SS-I), built by finite element modeling and validated as the newest and most accurate algorithm for the estimation of the non-linear in vivo biomechanical behavior in corneas with normal topography.[39]

However, and besides proven repeatability,[40,41] care needs to be taken in all these assumptions due to the lack of external validation in different populations and ocular status. In the present study, both glaucomatous groups within each pair (HMG and POAG) presented a biomechanical behavior compatible with less stiffer tissues. Moreover, the higher AUROCs to discriminate HMG and HMNG were found for DefAmpMax, HCDefoA, A2DL, HCDA, MaxDA, and HCDArea and to discriminate between POAG and NMNG eyes were found for A1dArcL, A2dArcL, MIR, DARM1, DARM2 and CBI, and these results are compatible with the trend of more significant information taken from the 2nd generation parameters within pair 2, but highlight the role of 1st generation basic corneal behavior descriptors in the myopia subset (pair 1).

The Whole Eye Movement (WEM) concept has to be appreciated as the accessory movement occurred beyond the 8mm diameter area. It is maximum near A2T and is expected to be lower in less stiff corneas, as more energy is absorbed and converted in movement in the center of these corneas with a low amount spreading to peripheral cornea.[35] The present study did not find statistical differences regarding these parameters.

Analyzing the logistic regression final models applied to each pair of groups and built to assess the effect of corneal biomechanics in the presence of glaucoma after adjustment for the interaction between all parameters, we can highlight some insights: the parameters were different when comparing the high myopia and non-myopia subsets; there were both 1st and 2nd generation parameters included in both models; the newest SS-I parameter was the only one present in both models; not all included parameters are in line with the aforementioned theoretical assumptions of the differential role of each one when analyzed alone, which proves the complexity of a biomechanical behavior integrated description; there is a possible less significant role of corneal thickness itself in relation to ocular biomechanical behavior in myopia subset, as its value was not significantly different between high myopia groups and proven additionally by the greater AUROC found in its purely biomechanical model without cCCT (0.947 VS 0.857).

When analyzing the final model applied to all of the 209 eyes to build a robust biomechanical tool of risk prediction for the presence of glaucoma with myopia interaction, the A1T, A2T, MaxDA, A1DArea, HCDArea, MIR, DARM1, and SS-I appeared as the most robust Corvis-derived parameters, with an overall AUROC of 0.917 and a sensitivity of 83% and specificity of 89% for the most upper left cut-off point of the curve.

Despite average similar VFI and number of current IOP lowering drops between HMG and POAG groups, the former presented lower ppRNFLT (mean and all sectors, $p < 0.05$ in all). However, the anatomic assessment in the HMG is challenging, which was highlighted by the proportion (62%) of exams with inaccurate or impossible segmentation within this group, lowering the accuracy in every statistical analysis. Due to the differential important role of structural changes

in early glaucomatous damage, those above plus the associated lack of normative data in high myopic patients limit the future utilization of the evolving anatomo-functional models to detect early glaucomatous damage in these eyes.

The unique characteristics of eyes with high myopia that limit structural assessment are the same giving rise to a possible differential role of an associated impaired ocular biomechanics in high myopia-associated glaucomatous damage. Thus, constructing a strong biomechanical model that can predict the risk of glaucoma development in these patients is well worth and is the main strength of this study. Additionally, the model can be applied to the prediction of damage progression and is currently being addressed in a different study by the same group, rendering it out of the scope of the present work. The authors consider the replication of this study with the Ocular Response Analyser® (ORA)[29] to be an added value in order to understand whether the results will be consistent.

The authors consider five possible limitations of this study which are explained below. First, both eyes of the same patient where included, however, this was done to maximize the data obtained in these relatively infrequent patients. Second, there is a lack of AL data within the non-myopic eyes but considering the similar and near emmetropic MRSE with no ocular history or other pathologies and considering the non-inclusion in the biomechanical models, it is not associated to final differences in the study outcomes. Second, excluding age from the biomechanical models could be understood as a limitation. However, as the relationship of age with corneal biomechanics is controversial and the SS-I is described with strong age association,[39] the possible introduction of this parameter in the models could limit the inferences on biomechanical properties alone. Third, the floor value of 25µm arbitrarily introduced in some OCT measurements in HMG group could be understood as a limitation, but the authors consider it the best way to highlight the aforementioned OCT-related issues in this group. Fourth, the Bruch's membrane opening minimum rim width (BMO-MRW) was not analysed in the present study as it will be analysed in another study from the same group.

Conclusion

In conclusion, both 1st and 2nd generation corneal biomechanical parameters measured through the Scheimpflug-camera technology demonstrated differences in eyes with glaucoma and biomechanical impairment demonstrated to be more associated with the presence of glaucoma in high myopic than in non-myopic eyes. The results are consistent with the stated hypothesis, as a biomechanical model based on logistic regression analysis and adjusted for high myopia could be built, with an overall probability of 91.7% (83% S and 89% E) for the correct prediction of glaucomatous damage. These results can validate the introduction of corneal biomechanical analysis by means of Scheimpflug image in the glaucoma risk assessment within the high myopic population.

Data Sharing Statement

The datasets generated during and/or analyzed during the current study are available from the corresponding author on reasonable request.

Statement of Ethics

The study adhered to the tenets of the Declaration of Helsinki. Approval was obtained from the "Departamento de Ensino, Formação e Investigação" (DEFI) of Centro Hospitalar e Universitário do Porto (nr: 130-DEFI-132-CE). The informed consent from the patients was waived due to the total anonymization and confidentiality of the data and the absence of detailed individual data.

Acknowledgments

The authors want to express gratitude to those who made this work possible and are not referred to as co-authors, mainly the residents and the technicians who performed the exams. Additionally, we also thank the participants of the study.

Funding

No funding or sponsorship was received for this study or publication of this article.

Disclosure

Prof. Dr. Renato Ambrósio Jr reports personal fees from OCULUS, during the conduct of the study. The authors report no other conflicts of interest in this work.

References

1. Tham YC, Li X, Wong TY, Quigley HA, Aung T, Cheng CY. Global prevalence of glaucoma and projections of glaucoma burden through 2040: a systematic review and meta-analysis. *Ophthalmology*. 2014;121(11):2081–2090. doi:10.1016/j.ophtha.2014.05.013
2. Kass MA, Heuer DK, Higginbotham EJ, et al. The ocular hypertension treatment study: a randomized trial determines that topical ocular hypotensive medication delays or prevents the onset of primary open-angle glaucoma. *Arch Ophthalmol*. 2002;120(6):701–713. doi:10.1001/archopht.120.6.701
3. Trivli A, Koliarakis I, Terzidou C, et al. Normal-tension glaucoma: pathogenesis and genetics. *Exp Ther Med*. 2019;17(1):563–574. doi:10.3892/etm.2018.7011
4. Strouthidis NG, Girard MJ. Altering the way the optic nerve head responds to intraocular pressure-a potential approach to glaucoma therapy. *Curr Opin Pharmacol*. 2013;13(1):83–89. doi:10.1016/j.coph.2012.09.001
5. Sigal IA, Ethier CR. Biomechanics of the optic nerve head. *Exp Eye Res*. 2009;88(4):799–807. doi:10.1016/j.exer.2009.02.003
6. Roberts MD, Sigal IA, Liang Y, Burgoyne CF, Downs JC. Changes in the biomechanical response of the optic nerve head in early experimental glaucoma. *Invest Ophthalmol Visual Sci*. 2010;51(11):5675–5684. doi:10.1167/iovs.10-5411
7. Roberts MD, Liang Y, Sigal IA, et al. Correlation between local stress and strain and lamina cribrosa connective tissue volume fraction in normal monkey eyes. *Invest Ophthalmol Visual Sci*. 2010;51(1):295–307. doi:10.1167/iovs.09-4016
8. Satekenova E, Ko MWL, Kim JR. Investigation of the Optic Nerve Head Morphology Influence to the Optic Nerve Head Biomechanics - Patient Specific Model. Conference proceedings: Annual International Conference of the IEEE Engineering in Medicine and Biology Society IEEE Engineering in Medicine and Biology Society Annual Conference; 2019:5370–5373. DOI: 10.1109/embc.2019.8856743.
9. Ethier CR. Scleral biomechanics and glaucoma--a connection? *Can J Ophthalmol*. 2006;41(1):9–12. doi:10.1016/s0008-4182(06)80060-8
10. Burgoyne CF, Downs JC, Bellezza AJ, Suh JK, Hart RT. The optic nerve head as a biomechanical structure: a new paradigm for understanding the role of IOP-related stress and strain in the pathophysiology of glaucomatous optic nerve head damage. *Prog Retinal Eye Res*. 2005;24(1):39–73. doi:10.1016/j.preteyeres.2004.06.001
11. Girard MJ, Suh JK, Bottlang M, Burgoyne CF, Downs JC. Biomechanical changes in the sclera of monkey eyes exposed to chronic IOP elevations. *Invest Ophthalmol Visual Sci*. 2011;52(8):5656–5669. doi:10.1167/iovs.10-6927
12. Yang H, Ren R, Lockwood H, et al. The connective tissue components of optic nerve head cupping in monkey experimental glaucoma part 1: global change. *Invest Ophthalmol Visual Sci*. 2015;56(13):7661–7678. doi:10.1167/iovs.15-17624
13. Grytz R, Meschke G, Jonas JB. The collagen fibril architecture in the lamina cribrosa and peripapillary sclera predicted by a computational remodeling approach. *Biomech Model Mechanobiol*. 2011;10(3):371–382. doi:10.1007/s10237-010-0240-8
14. Helmy H, Leila M, Zaki AA. Corneal biomechanics in asymmetrical normal-tension glaucoma. *Clin Ophthalmol*. 2016;10:503–510. doi:10.2147/opth.S93725
15. Jonas JB, Berenshtein E, Holbach L. Lamina cribrosa thickness and spatial relationships between intraocular space and cerebrospinal fluid space in highly myopic eyes. *Invest Ophthalmol Visual Sci*. 2004;45(8):2660–2665. doi:10.1167/iovs.03-1363
16. Jeoung JW, Yang H, Gardiner S, et al. Optical coherence tomography optic nerve head morphology in myopia I: implications of anterior scleral canal opening versus bruch membrane opening offset. *Am J Ophthalmol*. 2020;218:105–119. doi:10.1016/j.ajo.2020.05.015
17. Salomão MQ, Hofling-Lima AL, Faria-Correia F, et al. Dynamic corneal deformation response and integrated corneal tomography. *Indian J Ophthalmol*. 2018;66(3):373–382. doi:10.4103/ijo.IJO_831_17
18. Joda AA, Shervin MM, Kook D, Elsheikh A. Development and validation of a correction equation for Corvis tonometry. *Comput Meth Biomech Biomed Eng*. 2016;19(9):943–953. doi:10.1080/10255842.2015.1077515
19. Eliasy A, Chen KJ, Vinciguerra R, et al. Ex-vivo experimental validation of biomechanically-corrected intraocular pressure measurements on human eyes using the CorVis ST. *Exp Eye Res*. 2018;175:98–102. doi:10.1016/j.exer.2018.06.013
20. Chen KJ, Eliasy A, Vinciguerra R, et al. Development and validation of a new intraocular pressure estimate for patients with soft corneas. *J Cataract Refract Surg*. 2019;45(9):1316–1323. doi:10.1016/j.jcrs.2019.04.004
21. Anderson D, Chauhan B, Johnson C, Katz J, Patella V, Drance S. Criteria for progression of glaucoma in clinical management and in outcome studies. *Am J Ophthalmol*. 2001;130:827–829. doi:10.1016/S0002-9394(00)00665-6
22. Ehlers N, Bramsen T, Sperling S. Applanation tonometry and central corneal thickness. *Acta Ophthalmol*. 1975;53(1):34–43. doi:10.1111/j.1755-3768.1975.tb01135.x
23. Valbon BF, Ambrósio-Jr. R, Fontes BM, Alves MR. Effects of age on corneal deformation by non-contact tonometry integrated with an ultra-high-speed (UHS) Scheimpflug camera. *J Arquivos Brasile de Oftalmol*. 2013;76:229–232. doi:10.1590/S0004-27492013000400008
24. Orr JB, Zvirgzdina M, Wolffsohn J. The influence of age, ethnicity, eye/body size and diet on corneal biomechanics. *Invest Ophthalmol Visual Sci*. 2017;58(8):1131.
25. Asaoka R, Nakakura S, Tabuchi H, et al. The relationship between corvis ST tonometry measured corneal parameters and intraocular pressure, corneal thickness and corneal curvature. *PLoS One*. 2015;10(10):e0140385–e0140385. doi:10.1371/journal.pone.0140385
26. Ren R, Wang N, Li B, et al. Lamina cribrosa and peripapillary sclera histomorphometry in normal and advanced glaucomatous Chinese eyes with various axial length. *Invest Ophthalmol Visual Sci*. 2009;50(5):2175–2184. doi:10.1167/iovs.07-1429
27. Kimura Y, Akagi T, Hangai M, et al. Lamina cribrosa defects and optic disc morphology in primary open angle glaucoma with high myopia. *PLoS One*. 2014;9(12):e115313. doi:10.1371/journal.pone.0115313
28. Furlanetto RL, Park SC, Damle UJ, et al. Posterior displacement of the lamina cribrosa in glaucoma: in vivo interindividual and intereye comparisons. *Invest Ophthalmol Visual Sci*. 2013;54(7):4836–4842. doi:10.1167/iovs.12-11530
29. Kaushik S, Pandav SS. Ocular response analyzer. *J Curr Glaucoma Pract*. 2012;6(1):17–19. doi:10.5005/jp-journals-10008-1103

30. Tubtimthong A, Chansangpetch S, Ratprasatporn N, et al. Comparison of corneal biomechanical properties among axial Myopic, Nonaxial Myopic, and Nonmyopic eyes. *Biomed Res Int*. 2020;2020:8618615. doi:10.1155/2020/8618615
31. Wang J, Li Y, Jin Y, Yang X, Zhao C, Long Q. Corneal biomechanical properties in myopic eyes measured by a dynamic scheimpflug analyzer. *J Ophthalmol*. 2015;2015:1–8. doi:10.1155/2015/161869
32. Miki A, Yasukura Y, Weinreb R, et al. Dynamic scheimpflug ocular biomechanical parameters in untreated primary open angle glaucoma eyes. *Investigat Opthalmol Vis Sci*. 2020;61:19. doi:10.1167/iovs.61.4.19
33. Vinciguerra R, Rehman S, Vallabh NA, et al. Corneal biomechanics and biomechanically corrected intraocular pressure in primary open-angle glaucoma, ocular hypertension and controls. *J Br J Ophthalmol*. 2020;104(1):121–126. doi:10.1136/bjophthalmol-2018-313493
34. Salomão MQ, Hofling-Lima AL, Gomes Esporcatte LP, et al. The role of corneal biomechanics for the evaluation of ectasia patients. *Int J Environ Res Public Health*. 2020;17(6):2113. doi:10.3390/ijerph17062113
35. Jędzierowska M, Koprowski R. Novel dynamic corneal response parameters in a practice use: a critical review. *Biomed Eng Online*. 2019;18(1):17. doi:10.1186/s12938-019-0636-3
36. Valbon BR, Fontes B, Luz A, Roberts C, Alves M, Alves MR. Ocular biomechanical metrics by CorVis ST in healthy Brazilian patients. *J Refract Surg*. 2014;30:1–6. doi:10.3928/1081597X-20140521-01
37. Roberts C, Mahmoud A, Bons J, et al. Introduction of two novel stiffness parameters and interpretation of air puff–induced biomechanical deformation parameters with a dynamic scheimpflug analyzer. *J Refract Surg*. 2017;33:266–273. doi:10.3928/1081597X-20161221-03
38. Vinciguerra R, Ambrósio R, Elsheikh A, et al. Detection of keratoconus with a new biomechanical index. *J Refract Surg*. 2016;32(12):803–810. doi:10.3928/1081597x-20160629-01
39. Eliasy A, Chen KJ, Vinciguerra R, et al. Determination of corneal biomechanical behavior in-vivo for healthy eyes using CorVis ST tonometry: stress-strain index. *Front Bio Biotech*. 2019;7:105. doi:10.3389/fbioe.2019.00105
40. Bak-Nielsen S, Pedersen IB, Ivarsen A, Hjortdal J. Repeatability, reproducibility, and age dependency of dynamic Scheimpflug-based pneumotonometer and its correlation with a dynamic bidirectional pneumotonometry device. *Cornea*. 2015;34(1):71–77. doi:10.1097/ico.0000000000000293
41. Nemeth G, Hassan Z, Csutak A, Szalai E, Berta A, Modis L. Repeatability of ocular biomechanical data measurements with a Scheimpflug-based noncontact device on normal corneas. *J Refract Surg*. 2013;29(8):558–563. doi:10.3928/1081597x-20130719-06